



HAL
open science

Progress in the optical studies of single InGaN/GaN quantum dots

Anas François Jarjour, Rachel A. Oliver, Robert A. Taylor

► **To cite this version:**

Anas François Jarjour, Rachel A. Oliver, Robert A. Taylor. Progress in the optical studies of single InGaN/GaN quantum dots. *Philosophical Magazine*, 2007, 87 (13), pp.2077-2093. 10.1080/14786430701311219 . hal-00513827

HAL Id: hal-00513827

<https://hal.science/hal-00513827>

Submitted on 1 Sep 2010

HAL is a multi-disciplinary open access archive for the deposit and dissemination of scientific research documents, whether they are published or not. The documents may come from teaching and research institutions in France or abroad, or from public or private research centers.

L'archive ouverte pluridisciplinaire **HAL**, est destinée au dépôt et à la diffusion de documents scientifiques de niveau recherche, publiés ou non, émanant des établissements d'enseignement et de recherche français ou étrangers, des laboratoires publics ou privés.



Progress in the optical studies of single InGaN/GaN quantum dots

Journal:	<i>Philosophical Magazine & Philosophical Magazine Letters</i>
Manuscript ID:	TPHM-06-Jul-0258.R2
Journal Selection:	Philosophical Magazine
Date Submitted by the Author:	21-Feb-2007
Complete List of Authors:	Jarjour, Anas; University of Oxford, Physics Oliver, Rachel; University of Cambridge, Materials Science & Metallurgy Taylor, Robert; University of Oxford, Physics
Keywords:	localized states, photoluminescence, quantum dots
Keywords (user supplied):	InGaN, quantum confined stark effect, biexcitons



Progress in the optical studies of single InGaN/GaN quantum dots

Anas F. Jarjour[†], Rachel A. Oliver[‡], and Robert A. Taylor^{*†}

[†]Department of Physics, University of Oxford, Parks Road, Oxford, OX1 3PU, UK.

[‡]*Department of Materials, University of Cambridge, Pembroke Street, Cambridge CB2 3QZ, U.K*

*Corresponding author. Email: r.taylor1@physics.ox.ac.uk

Abstract

The great success that GaN-based structures have enjoyed in implementing efficient opto-electronic devices has fostered a rapidly expanding interest amongst researchers aimed at understanding their underlying physics. There has been an active debate on the mechanisms that give rise to efficient luminescence in these materials. In this paper we approach these questions through optical studies of single InGaN/GaN quantum dots in the context of the available experimental and theoretical understanding of InGaN structures in general, and of three-dimensional localization in this material in particular. We will also show how it is possible to exploit the various unique properties that nitride-based materials offer, such as the strong inbuilt electric field, in a controlled manner. Such control may in the future prove essential for the implementation of single quantum dot devices in applications such as quantum information processing. We also show how non-linear spectroscopy provides an invaluable tool in suppressing background luminescence effects inherent in this material.

Keywords: Quantum dots; InGaN; localized states ; Photoluminescence ; Quantum confined Stark effect ; Biexcitons.

1. Introduction

Nitride semiconductor structures have attracted much interest over the last decade because of their unique properties, which make them promising candidates for optoelectronic devices. Indeed, since the mid-1990s, InGaN quantum well (QW) structures have proven successful as active layers in high efficiency light-emitting diodes (LEDs) and laser diodes (LDs) [1] with the emission tuned from violet to green by changing the alloy composition. However, given the poor crystalline quality and the high threading dislocation density in these structures, such high quantum efficiency is surprising.

The origin of this bright luminescence has been generally attributed to the existence of localization centres or even quantum-dot-like states responsible for the suppression of the diffusion of carriers to the various non-radiative defects. The nature of these centres is somewhat controversial; suggestions include In-rich clusters and monolayer thickness fluctuations within the QW [2-4]. Since localization centres in InGaN are believed to play an essential role in enhancing the properties of devices, a great deal of work over the past decade has been devoted to the intentional fabrication and control of the properties of InGaN quantum dots (QDs). In particular, such structures could improve significantly the performance of optical devices such as lasers which are expected to have lower and temperature-independent threshold currents and narrower spectra when QDs are employed as the active medium [5].

One of the important properties that make GaN-based structures with wurtzite symmetry different from other materials is the large in-built electric field ($\sim \text{MVcm}^{-1}$). This field arises from both spontaneous polarization and piezoelectricity, with piezoelectric constants of nitride semiconductors being up to ten times larger than those of conventional III-V and II-VI compounds [6]. This field is believed to have a strong impact on device functionality as it causes a luminescence wavelength shift [7,8] and a reduction of the oscillator strength [9,10]. Furthermore, it has been predicted that this property, together with the high electron and hole effective masses, would make GaN-based QDs interesting candidates for quantum information processing (QIP) [11,12].

In this context we attempt in the present paper to review the advances in the understanding of the optical properties of single InGaN/GaN QDs. We have performed measurements on different InGaN QDs samples grown by various techniques. We relate our findings to other reported studies of intentionally-grown InGaN and other GaN-based QDs as well as measurements from localization centres in InGaN QWs.

2. Growth of InGaN/GaN QDs

Several techniques have been employed in the growth of InGaN/GaN QDs. Self-assembled QDs were grown using metalorganic chemical vapour deposition (MOCVD) [13,14] and molecular beam epitaxy (MBE) [15-17]. Whilst the mechanism of formation of InGaN nanostructures using MBE growth is commonly attributed to a 2D-to-3D transition in the well known Stranski-Krastanow mode, the mechanism associated with the MOCVD growth seems to be more complex and may involve phase separation.

While great control can be achieved over the statistical properties of self-assembled QDs, such as the areal density and the size, by a careful adjustment of the growth conditions, very little control over the QD position is possible. However, such

control is highly desirable for several applications involving QIP and QDs in high-Q microcavities. One method which overcomes this problem is selective growth. Several studies have reported the selective growth of site-controlled InGaN/GaN QDs [18-20]. In this technique, GaN micro-pyramids are grown by MOCVD through an array of holes lithographically patterned into a silica (SiO₂) mask on a GaN-on-sapphire substrate. Under appropriate conditions, due to the stability of the {10-10} planes in the wurtzite GaN crystal structure, hexagonal-based pyramids may be grown, which are then topped by InGaN/GaN QWs. Three-dimensional confinement is obtained at the apices of the pyramids, and the QWs formed on the facets of the pyramid are referred to as side QWs.

Measurements from three InGaN/GaN QD samples grown by different techniques are presented in this paper. Sample A contained self-assembled QDs and was grown by Arakawa *et al.* using MOCVD [13]. The average dot height is 5 nm and the average width is 23 nm. The areal density of QDs is $\sim 10^{10}$ cm⁻². Sample B was grown by Oliver *et al.* [14] by MOCVD; in this case, QD growth involved a post-growth anneal of the InGaN epilayer in molecular nitrogen prior to capping with GaN. The average dimensions of the dots are estimated to be 0.9 nm in height and 22 nm in diameter with an areal density of $\sim 10^{10}$ cm⁻². The QDs in these two samples are formed on top of a two-dimensional (2D) QW commonly referred to as a wetting layer (WL). Sample C consisted of arrays of selectively grown micro-pyramids topped by 5-periods of InGaN QWs of 2.0 nm thickness and GaN barriers of 6.0 nm thickness fabricated by Watson *et al.* [19]. The hexagonal-based pyramids were ~ 8 μ m in height with base edges of ~ 5 μ m and an areal density of 2×10^6 cm⁻². Cathodoluminescence measurements from this sample are reported in [19].

3. Single InGaN/GaN QD Spectroscopy

Spatially-resolved micro-photoluminescence (micro-PL) spectroscopy has proven to be a powerful technique in the study of QDs. Early work on InGaN/GaN QWs employed techniques such as scanning near-field optical microscopy (SNOM) [21,22], cathodoluminescence [23,24] and PL using nanoapertures [25]. However, these studies did not reveal the sharp spectral lines which are the signature of individual localisation centres. Recently, narrow spectral lines were observed in an InGaN/GaN QW, and were claimed to originate from single localized states [26]. Sharp spectral peaks were also observed in emission from intentionally grown InGaN QDs [27], where the linewidth was limited by the resolution of the experimental setup (170 μ eV); no sharp peaks were observed from an InGaN QW excited under the same conditions. These findings were qualitatively explained by the fact that the period of compositional fluctuations is estimated to be 20 nm and hence for a resolution of 100 nm, a large number of states are still probed. However, this explanation is in contrast with the results reported in [26] where such resolution is used. These dissimilar results might be due to differences in QW growth methodology, which could give rise to different distributions of localisation centres.

We have carried out spatially-resolved micro-PL measurements on the three samples mentioned above at 4.2 K. The carriers were excited above the GaN bandgap by either a HeCd laser (325 nm) or a frequency tripled 100-fs-pulsed Ti:sapphire laser (266 nm). The sample was mounted in a temperature-controlled cryostat and the laser was

1
2
3 focused by a $\times 36$ microscope objective to a spot size of $\sim 2 \mu\text{m}$. The PL was collected by
4 the same objective and directed to either a 0.3 m spectrograph with a 1200 grooves/mm
5 grating, giving a spectral resolution of $\sim 650 \mu\text{eV}$ or a double-grating 0.85 m spectrograph
6 with a resolution $\sim 100 \mu\text{eV}$. The spectrum was detected using a cooled CCD detector.
7 For samples A and B, the required spatial resolution was obtained by fabricating 200-
8 2000 nm square apertures (similar to the nanoapertures described in [25]) in a 100-nm-
9 thick Al layer deposited on the surface of the sample. As for sample C, it was possible to
10 resolve single QDs spatially due to the large separation between pyramids.
11
12

13 Figures 1(a)-(c) show typical micro-PL spectra from samples A-C, respectively.
14 Sharp narrow spectral lines are observed from the three samples which are clear evidence
15 of the existence of QDs. The QD emission is often observed to be superimposed onto a
16 strong background arising from the underlying wetting layer (WL) in samples A and B or
17 from the side QWs of the pyramids in sample C. Such strong background was also
18 observed in previous studies [27]. It should be mentioned that previous studies on
19 selectively-grown InGaN QDs did not report sharp peaks [18,20], but rather inferred the
20 existence of 3D-confinement in an indirect way. We observed significant variation of the
21 linewidth and the narrowest lines that we have measured are 290, 230 and 650 μeV for
22 samples A, B and C, respectively. It is well known that the measurement of the linewidth
23 gives an indirect measurement of the dephasing time T_2 ; a quantity of particular
24 importance for QIP applications. In fact, for the pure radiative limit the full-width-at-half-
25 maximum (FWHM) of the emission is related to the dephasing time by the equation
26 $\text{FWHM} = 2\hbar / T_2$. Therefore, the observed linewidths would correspond to dephasing
27 times of 4.5, 5.7 and 2.0 ps for the presented QDs. These values are more than one of
28 order of magnitude less than those measured from arsenide QDs [28]. However, as will
29 be shown in Section 3.2, other processes may be involved in the observed broadening and
30 hence, the mentioned dephasing times are only lower limits.
31
32
33
34

35 *3.1. Time-resolved measurements*

36
37 Several studies have examined recombination dynamics in ensembles of InGaN QDs
38 [2,29] and it was found that the decay traces exhibited non-exponential behaviour.
39 Several hypotheses were suggested to explain these results. It was proposed that this
40 would arise from recombination in heavily disordered material or simply from the
41 superposition of many exponential decays in the localization centres [29,30]. This was
42 also attributed to the existence of a fast process due to hopping of carriers between
43 different localized states and a slow process of recombination in those states [31]. Similar
44 behaviour was also found for ensembles of GaN/AlN QDs [32].
45
46

47 We have performed time-resolved measurements on single InGaN QDs using a
48 time-correlated single-photon-counting system based on a fast photomultiplier (PMT).
49 The PMT gave a time resolution of 150 ps. Figures 2(a) and 2(b) show time-integrated
50 spectra of QDs from samples A and B at 4.2 K. As mentioned previously, the QD
51 emission is superimposed on a strong background arising from the WL, hence the decay
52 trace recorded for a spectral window containing only the QD emission peak (traces
53 labelled QD+WL in figures 2(c) and 2(d)) would unavoidably have a contribution from
54 the emission of the WL. In order to extract the decay trace exclusively from the QD, we
55 measure that of the WL on both spectral sides of the QD emission and close to it, and
56
57
58
59
60

1
2
3 then these two traces are averaged and subtracted from that recorded at the QD. The
4 resulting traces are shown in figures 2(e) and 2(f).
5

6 While the decay trace from the WL exhibits non-exponential behaviour, it can be
7 seen clearly that a single exponential decay is observed from the InGaN QD with
8 lifetimes of 1.07 and 2.59 ns for samples A and B, respectively. These findings suggest
9 that the previously observed non-exponential behaviour is likely to be due to the
10 combination of QD and WL contributions. The temperature dependence of the PL and the
11 lifetime was investigated [33]. Quenching and broadening of the QD emission together
12 with a monotonic decrease of the lifetime with increasing temperature were found. This
13 indicates that non-radiative processes and/or escape of carriers become more and more
14 dominant.
15

16 A single-exponential decay was also obtained from QDs in sample C following this
17 subtraction method (figure 3) with a lifetime of 500 ps. Further evidence of this single-
18 exponential behaviour will be presented in Section 4 when no subtraction is necessary as
19 the background is totally suppressed.
20
21

22 **3.2. Spectral diffusion**

23

24 The local semiconductor environment in the vicinity of a QD may strongly influence its
25 energy levels. In particular, fluctuations in the local charge distribution lead to randomly-
26 varying electric fields which cause a slight stochastic shift of the QD energy level
27 (usually called spectral diffusion) via the quantum-confined Stark effect (QCSE). The
28 source of the fluctuating charge is widely attributed to charging and discharging of
29 nearby defects or interface states [34-36]. This phenomenon is therefore expected to be
30 pronounced in InGaN QDs because of the large density of defects present in the structure.
31 It can also provide an explanation for the broad linewidth usually observed.
32
33

34 We have investigated the temporal behaviour of the PL from single InGaN QDs
35 from sample B. This was done by recording consecutive spectra over 3000 s with
36 individual integration times of 3 s. Figure 4(a) shows the time evolution of emission line
37 from a single QD over 42 s and figure 4(b) shows the time evolution of the same line
38 over a longer time-scale. Fluctuations of the peak energy up to 0.3 meV are observed
39 over the short time- scale. This was accompanied with fluctuations in the linewidth of
40 150 μeV . Over the longer observation time, larger fluctuations of up to 1 meV in the peak
41 energy and 350 μeV in line width are found. These fluctuations are seen more clearly in
42 figures 4(c) and 4(d) where the energy and the linewidth of the QD emission are plotted
43 against the time. From auto-correlation calculations, we did not find any periodic
44 behaviour in these fluctuations. This is in contrast with what was reported for CdSe QDs
45 [34]. It is nevertheless consistent with the fact that spectral diffusion caused by electric
46 fields from locally trapped carriers would be expected to vary randomly with time.
47
48

49 Statistical histograms of the occupancy of an energy interval by the QD emission
50 throughout the time evolution are plotted in figure 1(e) for three different power
51 densities. At the highest power, one primary and one secondary maximum with energy
52 separation of 0.45 meV are observed. The secondary maximum may be due to carrier
53 dynamics in a nearby defect. The proximity of such a site may induce a shift of this
54 magnitude and occurring more frequently than that induced by more distant defects. As
55 would be expected, the secondary maximum disappears when the power density is
56
57
58
59
60

reduced since fewer carriers are excited and hence fewer trapping and un-trapping events occur. These findings give further evidence of the important role played by defects and localization centres even in intentionally grown InGaN QD structures.

3.3. Multi-excitonic complexes

The study of few-particle states in QDs is of particular importance, from a fundamental physics point of view, as it involves an understanding of the interrelation between Coulomb interactions and three-dimensional confinement. Moreover, the radiative decay of biexcitons in a QD is predicted [37] and demonstrated experimentally [38] to be a source of triggered polarization-entangled photon pairs.

Multi-excitonic complexes have been observed in micro-PL spectra from GaN/AlN self-assembled QDs [39] and from localized states in InGaN quantum wells [26, 40]. In these studies, the spectral lines arising from such complexes are identified from the dependence of the emission lines on the excitation power. The fundamental exciton peak (X) increases linearly while the biexciton peak (XX) exhibits a quadratic increase with the excitation power [41]. The binding energy of biexcitons, which is defined as the difference between the recombination energies of the exciton and the biexciton ($E_X - E_{XX}$), was reported to be ~ -5 meV [26], or even to vary between -3.4 and 16 meV [40]. Negative binding energies mean that the two excitons are in an anti-bound state. Such a state is usually not stable in bulk materials and it is only because of the effect of confinement in QDs that such a biexcitonic state can exist. In order to understand these findings, theoretical calculations have been carried out, in particular for nitride-based QDs [42]. In fact, the binding energy of biexcitons is given by:

$$E_X - E_{XX} \approx -(2J_{eh} + J_{ee} + J_{hh})$$

where J_{eh} is the electron-hole coulomb interaction which is negative, J_{ee} and J_{hh} are the electron-electron (e-e) and hole-hole (h-h) interactions which are positive. In nitride-based QDs, the strong inbuilt electric field leads to a spatial separation of the electron and the hole and hence $|J_{eh}|$ is expected to decrease significantly and the repulsive e-e and h-h interactions become dominant and lead to negative binding energies.

The recombination dynamics of multi-excitonic states also reveal important information on the quantum correlations among electrons and holes localized in the QD [43]. This can be achieved through time-resolved measurements of the recombination rates for the different states. From a simplistic point of view, the recombination rate of a biexciton should be twice that of an exciton as there are two paths by which it can take place. However, this seemingly intuitive picture neglects the interactions between the carriers. Indeed, such measurements, which have been made on several QD structures such as CdSe/ZnSe [44,45] and InGaAs QDs [46-49], revealed a ratio between the biexciton and the exciton recombination rates Γ_{XX} / Γ_X varying between 0.33 and 2.

We have studied the recombination dynamics of biexcitons in single InGaN QDs from sample A [50]. Figures 5(a) and 5(b) show micro-PL spectra recorded at 4.2 K from a single QD and the intensities of the two observed emission lines as a function of the excitation power densities. The measured energy of the X line is 2.825 eV and the binding energy of the XX line is observed to be -41 meV, indicating an anti-bound biexciton. Theoretical calculations of the wavefunctions and energies of excitons and biexcitons for QDs similar to those in our sample [42] resulted in an X energy of 2.819

1
2
3 eV and a XX binding energy of -51 meV. Thus good agreement is found, with
4 discrepancies between the theoretical and experimental values likely to be due to
5 uncertainties in the measured indium composition and/or the QD size. The other peaks
6 observed in the spectra may originate from other QDs present in the aperture.
7

8 Time-resolved spectra of the X and XX lines are presented in figures 5(c) and
9 5(d) for an excitation power of $3 \times 10^2 \text{ Wcm}^{-2}$ using the background subtraction method
10 previously presented. It is observed that the onset of the X decay curve is delayed, which
11 is explained by the refilling of the X state after the radiative decay of XX [44]. With this
12 taken into account, we obtain from the fit of the experimental data the lifetimes
13 $\tau_{XX} = 1.4 \pm 0.1 \text{ ns}$ and $\tau_X = 1.0 \pm 0.1 \text{ ns}$ and hence the ratio between the two
14 recombination rates $\Gamma_{XX} / \Gamma_X = 0.7$. Therefore, the interaction between the two excitons,
15 or rather the four localized fermions from which the anti-bound biexciton is formed, is
16 likely to be important.
17
18
19

20 **3.4. Quantum-confined Stark effect (QCSE)**

21
22 It was mentioned earlier that the QCSE modifies the energy of the optical transitions in a
23 QD, influencing the spatial separation between the localized electrons and holes. While
24 this effect exists intrinsically as a result of the inbuilt electric field and the charge
25 distribution in the vicinity of the QD, it can be exploited in a controlled manner by
26 applying external electric fields. This property can prove important for numerous
27 applications such as ultrafast electro-optical modulators. Indeed, QCSE applied to QWs
28 has been used to fabricate such devices [51]. However, QDs have the additional
29 advantage of tunability with ultra-narrow bandwidths. Such control is also highly
30 desirable for QIP-related applications [52].
31
32

33 From a fundamental physics point of view, study of the Stark effect provides
34 important information on the carrier wave functions. It has been shown [53] that if the
35 QD possesses a permanent dipole, the energy shift induced by the applied field has a
36 linear component as well as the usual quadratic component arising from the
37 polarizability. Such a permanent dipole is induced by the spatial separation between the
38 electron and hole wave functions. As explained previously, this is likely to be the case in
39 GaN-based QDs because of the inbuilt electric field.
40

41 The effects of both lateral and vertical applied electric fields with respect to the
42 QD plane have been studied in several QD structures [54-56]. However, only a few
43 recent studies have reported such measurements on GaN/AlN [57,58] and InGaN/GaN
44 QDs [59,60]. It was found that a vertical electric field can result in an almost linear blue
45 shift of the optical transition of up to 100 meV in GaN/AlN QDs [58] due to the partial
46 compensation of the in-built field and the dominant effect from the induced permanent
47 dipole. The accompanied increase of the overlap between the electron and hole wave
48 functions leads to an increase of the binding energy up to 1 meV.
49

50 We have investigated the effect of an applied lateral electric field on the optical
51 properties of single self-assembled InGaN/GaN QDs from a sample similar to B, which
52 consisted of dots formed on 10 monolayers of InGaN and capped by 7 nm of GaN. A
53 100-nm-thick pair of Al electrodes was fabricated on the surface of the sample with a
54 separation of 1 μm . For a bias of 10 V between the two electrodes, the lateral component
55 of the field varies between a minimum of 0.065 MVcm^{-1} and a maximum of 0.18
56
57
58
59
60

MVcm⁻¹. Micro-PL measurements were carried out using the same experimental arrangement described previously.

Figure 6(a) shows micro-PL spectra from a spatially-resolved single dot, recorded at 4.2 K as a function of the applied voltage. It is seen that the peak undergoes a red-shift, reduction of the PL intensity and an increase in the linewidth with increasing bias. The red-shift can be readily explained by the QCSE in the lateral direction and the decrease in the PL intensity can be understood in terms of the reduction of oscillator strength due to the enhanced spatial separation between the electron and the hole. However, the observed broadening of the emission line suggests that field-induced carrier tunnelling is also present. This process has been observed in other QD systems [61] and has been proposed as an additional mechanism responsible for the decrease in the peak intensity.

In figure 6(b) the energy shift as obtained from a fit of the QD emission peak is plotted as a function of the calculated field strength and this energy shift is reproduced in the inset for low field strength. In the absence of a permanent dipole, the QCSE is expected to result only in a red shift of the exciton energy. However, it is observed from the inset of figure (b) that the QD energy undergoes a blue shift for applied fields up to ~0.04 MV/cm and a red shift for higher fields. This can only be explained by the compensation of the internal lateral piezoelectric field by the external field and hence reveals the existence of a lateral permanent dipole.

The experimental data are fitted with the equation

$$\Delta E(F) = \mu F + \alpha F^2.$$

As mentioned above, the linear contribution is related to a permanent dipole with μ being its lateral component and the quadratic term is related to a lateral component of the polarizability α . We obtain the values of $\mu = -1.52 \times 10^{-28}$ Cm and hence a non-vanishing lateral component of the dipole. This value would correspond to 0.95 nm in cgs units and is slightly larger than the value of 0.23 nm obtained from a linear fit of the blue shift presented in the inset. Such small separation between the electron and the hole in the lateral direction would be expected as it would arise from asymmetries in the QD shape and/or the alloy distribution. The fit gives a lateral component of the polarizability $\alpha = -1.45 \times 10^{-3}$ meV(kV)⁻²cm² or 20.7 nm³ in cgs units. This value is of the same order as that obtained for CdSe/ZnSe QDs [56]. It leads to a characteristic lateral dimension of the QD of 2.7 nm which is consistent with the value inferred below from the analysis of the linewidth broadening.

Figure 6(c) shows the dependence of the FWHM of the QD emission as a function of the applied field. Tunnelling-induced broadening of the QD spectral line under an electric field F can be modelled by [61]:

$$\text{FWHM} = \frac{\pi \hbar^2}{2m^* a^2} \exp\left(-\frac{4\sqrt{2m^*} V_0^{3/2}}{3\hbar e F}\right)$$

where a is the characteristic dimension of the QD, V_0 is the energy offset between the ground state of the electron and the lateral barrier, and m^* is the effective electron mass, which is estimated assuming 20% indium composition and averaging between the value of m^* for GaN (0.2 m_e) and for InN (0.042 m_e). Tunnelling of holes can be neglected due to their large effective mass. A fit to the experimental data gives the diameter of the QD as 2.1 nm, which is in fair agreement with AFM measurements, although rather on the

1
2
3 small side, and an energy offset of 9.51 meV. This shallow confinement potential can be
4 explained by the nature of the QDs in this sample as indium-rich InGaN islands on a
5 damaged WL.
6

8 **4. Nonlinear excitation of single InGaN/GaN QDs**

9
10 Nonlinear spectroscopy has been employed in the study of low-dimensional
11 semiconductor structures. For example, two-photon absorption (TPA) has been
12 investigated in QWs [62], quantum wires [63] and ensembles of semiconductor
13 nanocrystals in a glass matrix [64]. In fact, this technique provides the possibility of
14 exciting transitions that are forbidden for one-photon excitation (OPE). It is also useful
15 from a practical point of view as it enables a wide separation between the excitation and
16 detection wavelengths. In the present study, the term “nonlinear excitation” (NE) is used
17 for the process whereby the excitation energy falls in the bandgap of the structure, and
18 hence only transitions by multiple-photon absorption are possible. In our experiments,
19 this is achieved using 1-ps pulses from a tuneable Ti:sapphire laser with tuning resolution
20 of ~1.5 meV and employing the same micro-PL setup described previously.
21

22
23 First, we present in figures 7(a) and 7(b) micro-PL spectra under OPE obtained by
24 frequency-doubling the laser at excitation energy of 3.37 and 3.15 eV for samples B and
25 C, respectively. It should be noted that this energy is below the bandgap of GaN and
26 hence carriers should be excited directly into the QW to which the QDs are coupled. In
27 fact, it can be argued that the previously observed strong background might be due to the
28 large number of excited carriers which can diffuse to different lower-lying states in the
29 WL or side QWs under above-GaN-bandgap excitation. However, it is clear from the
30 spectra that a strong background is still observed.
31

32
33 In figures 7(c) and 7(d), micro-PL spectra under NE at an excitation energy of
34 1.55 eV are shown. A total suppression of the background emission from the QW is
35 observed in both cases and yet relatively strong QD emission is still seen. The line
36 present at 3.1 eV in figure 7(d) originates from the second-harmonic of the laser
37 generated inside the sample. Previous studies suggested that second-harmonic generation
38 (SHG) can be an additional absorption mechanism [63, 65]. However, if this mechanism
39 had an important role, it would have lead to similar results to those seen under OPE, i.e.
40 the observation of emission from the QW. Furthermore, we have carried out the same
41 measurements on a sample with only a planar InGaN/GaN QW, similar to the WL of
42 sample B, but no emission was observed under NE for the same range of intensities.
43 These findings can be explained qualitatively by the enhancement of the nonlinear
44 absorption cross-section in QDs due to the zero-dimensional confinement of carriers
45 compared to that of QWs. Time-resolved decay traces from the measured QDs are
46 presented in figures 7(e) and 7(f) without any subtraction procedure. They fit very well
47 with a single-exponential equation. This confirms unambiguously the mono-exponential
48 behaviour found previously by subtracting the WL contribution.
49

50
51 We have examined the dependence of the QD emission on the NE wavelength at a
52 fixed power in order to probe the existence of excited states. In fact, it would be expected
53 that when the energy of multiple photons correspond to the energy of an excited state, an
54 enhancement of the nonlinear absorption should occur. Figure 8 presents the results
55 obtained from the two QDs shown in figure 7. First, a broad absorption is observed 302
56
57
58
59
60

meV and 274 meV above the QD energy in samples B and C, respectively. This peak is observed for several QDs in both samples and is attributed to absorption of continuum states. Moreover, a resonance peak is observed for sample B at 149 meV above the QD and several resonance peaks are observed for sample C at energy separation from the QD of 73, 27 and -18 meV. Previous theoretical studies on hexagonal InGaN QDs report a separation between the first excited states and the ground state of 122 meV [66]. The modelled dot was bigger than those in sample B and smaller than those in sample C. Therefore, it is consistent to assign the peak at 149 meV for sample B and that at 73 meV for sample C to excited states. In this discussion, we have omitted the role of selection rules in this absorption. In fact, it should be mentioned that, due to valence-band mixing and the asymmetry of the QDs, the polarization states of the different energy levels in the QDs can differ from the two circularly-polarized states which are the eigenstates of the total angular momentum in a structure with rotational symmetry [67], and hence the selection rules become more complex. Future experiments to further understand these findings are under consideration.

When analysing the order of the non-linearity, it is important to investigate the intensity dependence of the QD emission on the NE power. This dependence is presented in figures 9(a) and 9(b) for the QDs presented in figure 7 from samples B and C, respectively. For sample B, only non-resonant excitation at 1.55 eV is examined. For sample C, two excitation energies are examined: at 1.55 eV (non-resonant excitation) and at 1.39 eV (resonant excitation corresponding to the state 73 meV above the dot). All the experimental data are fitted with the law:

$$I_{\text{QD}} = I_{\text{sat}} \left[1 - \exp \left[- \left(P / P_{\text{sat}} \right)^d \right] \right]$$

which corresponds to a multiple-order Poissonian absorption process. The best fit to the experimental data with the above law gives the following values: for sample B, 4.51 ± 0.58 and for sample C 4.40 ± 0.58 under non-resonant excitation and 2.96 ± 0.21 under resonant excitation. In order to eliminate the possibility that these indices arose from some artifact in the system, the intensity of the SHG line as a function of the excitation power was measured. The inset in figure 9(b) shows, on a logarithmic scale, a linear function corresponding to a power law $I_{\text{SHG}} = AP^d$ fitted to the second harmonic intensity. The fit gives $d = 2.06 \pm 0.13$, and hence the expected quadratic behaviour. It was previously found for quantum wells and quantum wires that the PL followed a quadratic dependence on the excitation power under NE [63,64] suggesting a two-photon absorption process. These findings indicate that higher order processes are involved in the NE in these dots. The slightly lower order under resonant excitation in Sample C is consistent with the assignment of this state as a p-state of the same QD. However, further experimental and theoretical work is needed in order to understand these findings fully.

5. Conclusion

In this study, we presented a review of the various optical properties of single InGaN/GaN quantum dots grown by different techniques. We have observed sharp spectral peaks which are clear evidence of the intentional three-dimensional confinement in this material. However, we showed that the particular environment of the InGaN structures leads to the observation of a strong background emission and to the broadening of the dot emission. This indicates stronger interaction between the confined carriers in

InGaN QDs and their local environment when compared to quantum dot structures in other materials systems. We have also revealed the existence of multi-excitonic states in InGaN dots and presented their related dynamics. Measurements under applied lateral electric fields revealed evidence of a lateral permanent dipole moment, probably due to the spatial separation between the electron and the hole in the dot. This field also enabled the exciton energy to be tuned. Non-linear spectroscopy was undertaken and resulted in total suppression of the strong background arising from the underlying quantum well. This enabled an initial observation of p-states. It is clear that further experimental work and theoretical modeling is still required to completely understand these findings with the aim of exploiting fully the rich possibilities that nitride-based structures may offer. In particular, the observed mono-exponential decay indicates that nitride QDs may have potential to act as blue single photon sources. Furthermore, the sharp QD emission observed from site-controlled QDs is promising as vertically-stacked QDs can be easily achieved in such structures. This may lead to systematic interactions between QDs possibly via the inbuilt electric field, which might prove interesting for QIP-related applications.

Acknowledgements

This research is part of the QIP IRC (www.qipirc.org) supported by EPSRC (GR/S82176/01). We also acknowledge funding from the Clarendon Fund and the ORS scheme (AFJ), and from Peterhouse, Cambridge (RAO).

References

- [1] S. Nakamura and G. Fasol, *The Blue Laser Diode*, (Springer-Verlag, Berlin, Germany, 1997).
- [2] I. L. Krestnikov, N. N. Ledentsov, A. Hoffmann, D. Bimberg, A. V. Sakharov, W. V. Lundin, A. F. Tsatsulnikov, A. S. Usikov, Z. I. Alferov, Y.G. Musikhin, and D. Gerthsen, *Phys. Rev.* **B 66** 155310 (2002).
- [3] D. Gerthsen, B. Neubauer, A. Rosenauer, T. Stephan, H. Kalt, O. Schon and M. Heuken, *Appl. Phys. Lett.* **79** 2552 (2001).
- [4] S. Chichibu et al, *J. Vac. Sci. Technol.* **B 16** 2204 (1998).
- [5] Y. Arakawa, *IEEE J. Sel. Topics in Quantum Electronics* **8** 823 (2002).
- [6] F. Bernardini, V. Fiorentini, and D. Vanderbilt, *Phys. Rev.* **B 56** R10024 (1997).
- [7] T. Takeuchi, S. Sota, M. Katsuragawa, M. Komori, H. Takeuchi, H. Amano, and I. Akasaki, *Jpn. J. Appl. Phys., Part 2* **36** L382 (1997).
- [8] S. Chichibu, T. Azuhata, T. Sota, and S. Nakamura, *Appl. Phys. Lett.* **69** 4188 (1996).
- [9] J. S. Im, H. Kollmer, J. Off, A. Sohmer, F. Scholz, and A. Hangleiter, *Phys. Rev.* **B 57** R9435 (1998).
- [10] T. Deguchi, K. Sekiguchi, A. Nakamura, T. Sota, R. Matsuo, S. Chichibu, and S. Nakamura, *Jpn. J. Appl. Phys., Part 2* **38** L914 (1999).
- [11] S. De Rinaldis, I. D'Amico, and F. Rossi, *Phys. Rev.* **B 69** 235316 (2004).
- [12] I. D'Amico, and F. Rossi, *Appl. Phys. Lett.* **81** 5213 (2002).
- [13] K. Tachibana, T. Someya, and Y. Arakawa, *Appl. Phys. Lett.* **74** 383 (1999).
- [14] R. A. Oliver, G. A. D. Briggs, M. J. Kappers, C. J. Humphreys, S. Yasin, J. H. Rice, J. D. Smith, and R. A. Taylor, *Appl. Phys. Lett.* **83** 755 (2003).
- [15] B. Daudin, G. Feuillet, G. Mula, H. Marriette, J. L. Rouviere, N. Pelekanos, G. Fishman, C. Adelman, and J. Simon, *Phys. Status Solidi A* **176** 621 (1999).
- [16] B. Daudin, N. Grandjean, F. Semond, J. Massies, and M. Leroux, *Appl. Phys. Lett.* **75** 962 (1999).
- [17] C. Adelman, J. Simon, G. Feuillet, N. T. Pelekanos, B. Daudin, and G. Fishman, *Appl. Phys. Lett.* **76** 1570 (2000).

- 1
2
3
4
5
6
7
8
9
10
11
12
13
14
15
16
17
18
19
20
21
22
23
24
25
26
27
28
29
30
31
32
33
34
35
36
37
38
39
40
41
42
43
44
45
46
47
48
49
50
51
52
53
54
55
56
57
58
59
60
- [18] K. Tachibana, T. Someya, S. Ishida, and Y. Arakawa, Appl. Phys Lett. **76** 3212 (2000).
[19] P. R. Edwards, R. W. Martin, I. M. Watson, C. Liu, R. A. Taylor, J. H. Rice, J. H. Na, J. W. Robinson, and J. D. Smith, Appl. Phys. Lett. **85** 4281 (2004).
[20] V. Perez-Solorzano, A. Groning, M. Jetter, T. Riemann, and J. Christen, Appl. Phys. Lett. **87** 163121 (2005).
[21] P. A. Crowell, D. K. Young, S. Keller, E. L. Hu, and D. D. Awschalom, Appl. Phys. Lett. **72** 927 (1998).
[22] A. Vertikov, A. V. Nurmikko, K. Doverspike, G. Bulman, and J. Edmond, Appl. Phys. Lett. **73** 493 (1998).
[23] X. Zhang, D. H. Rich, J. T. Kobayashi, N. P. Kobayashi, and P. D. Dapkus. Appl. Phys. Lett. **73** 1430 (1998).
[24] S. Chichibu, K. Wada, and S. Nakamura, Appl. Phys. Lett. **71** 2346 (1997).
[25] H. Yu, H. Htoon, A. deLozanne, C. K. Shih, P. A. Grudowski, R. D. Dupuis, K. Zeng, R. Mair, J. Y. Lin, and H. X. Jiang. J. Vac. Sci. Technol. B **16** 2215 (1998).
[26] H. Schomig, S. Halm, A. Forchel, G. Bacher, J. Off, and F. Scholz, Phys. Rev. Lett. **92** 106802 (2004).
[27] O. Moriwaki, T. Someya, K. Tachibana, S. Ishida, and Y. Arakawa, Appl. Phys. Lett. **76** 2361 (2000).
[28] C. Kammerer, G. Cassabois, C. Voisin, M. Perrin, C. Delalande, Ph. Roussignol and J. M. Gerard. Appl. Phys. Lett. **81** 2737 (2002).
[29] A. Morel, M. Gallart, T. Taliercio, P. Lefebvre, B. Gil, J. Allegre, H. Mathieu, B. Damilano, N. Grandjean, and J. Massies, Phys. Stat. Sol. A **180** 375 (2000).
[30] G. Mauckner, K. Thonke, T. Baier, T. Walter, and R. Sauer, J. of Appl. Phys. **75** 4167 (1994).
[31] S.-W. Feng, Y.-C. Cheng, Y.-Y. Chung, C. C. Yang, Y.-S. Lin, C. Hsu, K.-J. Ma, J.-I. Chyi, J. of Appl. Phys. **92** 4441 (2002).
[32] J. Simon, E. Martinez-Guerrero, C. Adelman, G. Mula, B. Daudin, G. Feuillet, H. Mariette, and N.T. Pelekanos, Phys. Stat. Sol. (b) **224** 12 (2001).
[33] J.W. Robinson, J.H. Rice, A. Jarjour, J.D. Smith, R.A. Taylor, R.A. Oliver, G.A.D. Briggs, M.J. Kappers, C.J. Humphreys, and Y. Arakawa, Appl. Phys. Lett. **83** 2674 (2003).
[34] J. Seufert, R. Weigand, G. Bacher, T. Kummell, A. Forchel, K. Leonardi and D. Hommel, Appl. Phys. Lett. **76** 1872 (2000).
[35] V. Turck, S. Rodt, O. Stier, R. Heitz, U. W. Pohl, R. Engelhardt and D. Bimberg, J. Lumin. **87** 337 (2000).
[36] H. D. Robinson and B. B. Goldberg, Phys. Rev. **B 61** 5086 (2000).
[37] O. Benson, C. Santori, M. Pelton, and Y. Yamamoto, Phys. Rev. Lett. **84** 2513 (2000).
[38] R. M. Stevenson, R. J. Young, P. Atkinson, K. Cooper, D. A. Ritchie and A. J. Shields. Nature **439** 179 (2006).
[39] S. Kako, K. Hoshino, S. Iwamoto, S. Ishida and Y. Arakawa, Appl. Phys. Lett. **85** 64 (2004).
[40] R. Seguin, S. Rodt, A. Strittmatter, L. Reissmann, T. Bartel, A. Hoffmann, D. Bimberg, E. Hahn and D. Gerthsen, Appl. Phys. Lett., **84** 4023 (2004).
[41] M. Grundmann and D. Bimberg, Phys. Rev **B 55** 9740 (1997).
[42] D. P. Williams, A. D. Andreev, D. A. Faux and E. P. O'Reilly, Physica E **21** 358 (2004).
[43] M. Wimmer, S. V. Nair, and J. Shumway, Phys. Rev. **B 73** 165305 (2006).
[44] G. Bacher, R. Weigand, J. Seufert, V. D. Kulakovskii, N. A. Gippius, A. Forchel, K. Leonardi, and D. Hommel, Phys. Rev. Lett. **83** 4417 (1999).
[45] B. Patton, W. Langbein, and U. Woggon, Phys. Rev. **B 68** 125316 (2003).
[46] C. Santori, G. S. Solomon, M. Pelton, and Y. Yamamoto, Phys. Rev. **B 65** R073310 (2002).
[47] R.M. Thompson, R. M. Stevenson, A. J. Shields, I. Farrer, C. J. Lobo, D. A. Ritchie, M. L. Leadbeater, and M. Pepper, Phys. Rev. **B 64** R201302 (2001).
[48] S. M. Ulrich, M. Benyoucef, P. Michler, N. Baer, P. Gartner, F. Jahnke, M. Schwab, H. Kurtze, M. Bayer, S. Fafard, Z. Wasilewski, and A. Forchel, Phys. Rev. **B 71** 235328 (2005).
[49] S. Kono, A. Kirihara, A. Tomita, K. Nakamura, J. Fujikata, K. Ohashi, H. Saito, and K. Nishi, Phys. Rev. **B 72** 155307 (2005).
[50] J.H. Rice, J.W. Robinson, J.H. Na, K.H. Lee, R.A. Taylor, D.P. Williams, E.P. O'Reilly, A.D. Andreev, Y. Arakawa and S. Yasin, Nanotechnology **16** 1477 (2005).
[51] D.A. Miller, *Confined Excitons and Photons*, (Plenum, New York, 1995), p. 675.
[52] H. J. Krenner, M. Sabathil, E. C. Clark, A. Kress, D. Schuh, M. Bichler, G. Abstreiter, and J. J. Finley. Phys. Rev. Lett. **93** 217401 (2004).

- 1
2
3 [53] P. W. Fry, I. E. Itskevich, D. J. Mowbray, M. S. Skolnick, J. J. Finley, J. A. Barker, E. P. O'Reilly, L.
4 R. Wilson, I. A. Larkin, P. A. Maksym et al., Phys. Rev. Lett. **84** 733 (2000).
5 [54] W. Heller, U. Bockelmann and G. Abstreiter, Phys. Rev. **B 57** 6270 (1998).
6 [55] S. Raymond, J. P. Reynolds, J. L. Merz, S. Fafard, Y. Feng and S. Charbonneau, Phys. Rev. **B 58**
7 13415 (1998).
8 [56] J. Seufert, M. Obert, M. Scheibner, N. A. Gippius, G. Bacher, A. Forchel, T. Passow, K. Leonardi and
9 D. Hommel, Appl. Phys. Lett. **79** 1033 (2001).
10 [57] T. Nakaoka, S. Kako, and Y. Arakawa, Phys. Rev **B 73** 121305(R) (2006).
11 [58] T. Nakaoka, S. Kako, and Y. Arakawa, Physica E **32** 148 (2006).
12 [59] J.W. Robinson, J.H. Rice, K.H. Lee, J.H. Na, R.A. Taylor, D.G. Hasko, R.A. Oliver, M.J. Kappers,
13 C.J. Humphreys, and G.A.D. Briggs, Appl. Phys. Lett. **86** 213103 (2005).
14 [60] B. Sherliker, M. P. Halsall, P. D. Buckle, P. J. Parbrook and T. Wang, Appl. Phys. Lett. **88** 122115
15 (2006).
16 [61] J. Seufert, M. Obert, M. Rambach, G. Bacher, A. Forchel, T. Passow, K. Leonardi, D. Hommel,
17 Physica E **13** 147 (2002).
18 [62] R. Cingolani and K. Ploog, Adv. Phys. **40** 535 (1991).
19 [63] R. Cingolani, M. Lepore, R. Tommasi, I. M. Catalano, H. Lage, D. Heitmann, K. Ploog, A. Shimizu,
20 H. Sakaki, and T. Ogawa, Phys. Rev. Lett. **69** 1276 (1992).
21 [64] K. I. Kang, B. P. McGinnes, Sandalphon, Y. Z. Hu, S. W. Koch, N. Peyghambarian, A. Mysyrowicz,
22 L. C. Liu and S. H. Risbod, Phys. Rev. **B 45** 3465 (1992).
23 [65] S.S. Jha, Phys. Rev. **145** 500 (1966).
24 [66] T. Saito, Y. Arakawa, Physica E **15** 169 (2002).
25 [67] M. Henini, S. Sanguinetti, S.C. Fortina, E. Grilli, and M. Guzzi, Phys. Rev. **B 57** R6815 (1998).
26
27
28
29
30
31
32
33
34
35
36
37
38
39
40
41
42
43
44
45
46
47
48
49
50
51
52
53
54
55
56
57
58
59
60

Figure Captions:

Figure 1. Micro-PL spectra from (a) sample A (b) sample B and (c) sample C under excitation above the bandgap of GaN. The spectra reveal narrow sharp lines originating from the recombination in QDs. The spectra are recorded at 4.2 K.

Figure 2. (a) and (b) are micro-PL spectra from single QDs in samples A and B, respectively. The QD is observed to be superimposed onto a strong background originating from the WL. (c) and (d) are time-resolved spectra plotted on a logarithmic scale corresponding to the QDs shown in (a) and (b), respectively. The spectrum labelled QD+WL is recorded for a spectral window containing only the QD line, while the spectrum labelled WL is the average of two spectra recorded on both spectral sides of the QD emission and close to it. (e) and (f) are the result of subtraction of the two spectra in (c) and in (d) in order to extract the decay trace exclusively from the QDs. A mono-exponential decay trace is obtained with lifetimes of 1.07 and 2.59 ns for samples A and B, respectively. These measurements are made at 4.2 K.

Figure 3. Time-integrated and time-resolved (on a logarithmic scale) spectra from single site-controlled QD at 4.2 K. The decay trace is obtained by applying the subtraction method mentioned in the text. In this case also, the decay is well described by a single exponential behaviour with lifetime of 500 ps.

Figure 4. Series of consecutively recorded micro-PL spectra from single QD in sample B at (a) 3s intervals and (b) 60s intervals. The time evolution of (c) the relative peak energy and (d) the linewidth of the QD emission line. It is observed that the QD emission undergoes spectral diffusion characterized by random fluctuations of the measured quantities. (e) Statistical histogram plots of the occupancy of each energy interval by the QD emission line, at three different power densities. A secondary maximum is observed for the highest power at -0.45meV from the main peak and gradually disappears for lower power densities.

Figure 5. (a) Micro-PL spectra recorded at 4.2K as a function of the power density. X line corresponds to single exciton and the XX lines to a biexciton. (b) A plot of the intensity of the X and XX lines as a function of the power density on a log-log scale. The fit reveals a linear increase of the X intensity and a quadratic dependence of the XX line on the power density as expected. (c) Decay trace of the X line whose life time is observed to be ~ 1 ns. (d) Decay trace of the XX line with lifetime of ~ 1.4 ns. Both are taken for a power density of 300 Wcm^{-2} . A significant rise time is observed for the X decay which is due to the filling from the XX state.

Figure 6. (a) A series of sequential micro-PL spectra from single QD recorded at 4.2 K with increasing voltage from 0 to 10 V. The integration time is 10 s for each spectrum. (b) Plot of the energy of the QD emission as a function of field strength. The data were fitted by a second order polynomial revealing the existence of lateral dipole moment. **The inset shows a close look at the energy shift for low field strength. A clear blue shift is observed for applied fields up to 0.04 MV/cm which can only be explained by the existence of a lateral permanent dipole.** (c) The linewidth of the QD emission as a function of the field. The broadening is fitted an electric field-induced tunnelling model.

Figure 7. Micro-PL spectra under OPE for several excitation powers for (a) sample B and (b) sample C. The excitation energies are 3.37 and 3.15 eV for sample B and C, respectively. Micro-PL spectra under NE

1
2
3 as a function of the excitation power for (c) sample B and (d) sample C. The excitation energy is 1.55 eV
4 for both samples. The spectra have been offset for clarity. Time-resolved decay curves for (e) the QD in
5 sample B at energy 2.86eV and (f) for the QD in sample C at 2.71 eV. The excitation powers were 20 and
6 56 mW, respectively. Both decay curves fit very well with single exponential giving lifetimes of $1.79 \pm$
7 0.03 ns and 947 ± 4 ps for samples B and C, respectively.
8

9
10 Figure 8. Non-linear PL excitation (PLE) spectra from the same QDs presented in figure 7. Each point
11 corresponds to the intensity of the QD emission at excitation energy of two-photons. The zero of the energy
12 scale is the energy of the corresponding QD. The excitation power is kept constant (20 mW and 50 mW for
13 sample B and C, respectively). The PL spectra from figure 7 are also shown for comparison (at 20 and 56
14 mW for B and C, respectively).

15 Figure 9. The intensity dependence of the QD emission on the excitation power (log-log scale). Sample B:
16 the excitation energy is 1.55 eV. Sample C: the square symbols correspond to excitation energy of 1.55 eV
17 and the triangular symbols to 1.39 eV. The continuous lines are the best fit of the experimental data with
18 the law $I_{\text{QD}} = I_{\text{sat}} [1 - \exp[-(P/P_{\text{sat}})^d]]$. The inset shows the intensity dependence of the second-harmonic
19 generated wave on the excitation power.
20
21
22
23
24
25
26
27
28
29
30
31
32
33
34
35
36
37
38
39
40
41
42
43
44
45
46
47
48
49
50
51
52
53
54
55
56
57
58
59
60

Figure 1

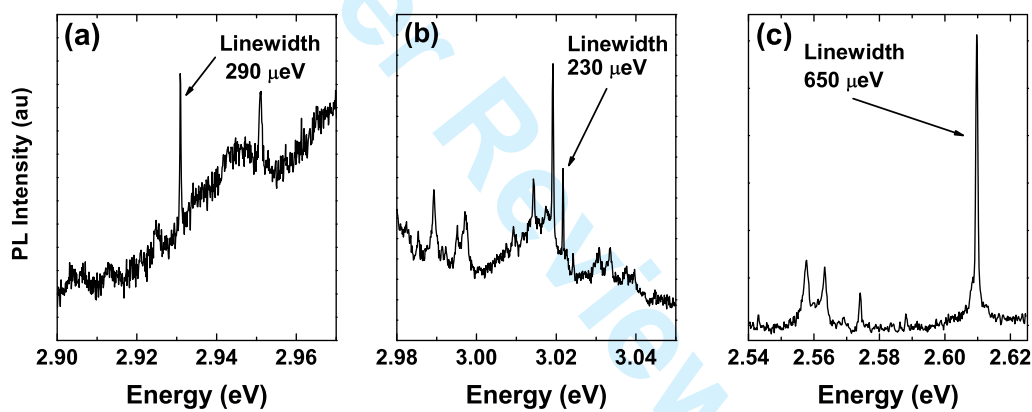


Figure 2

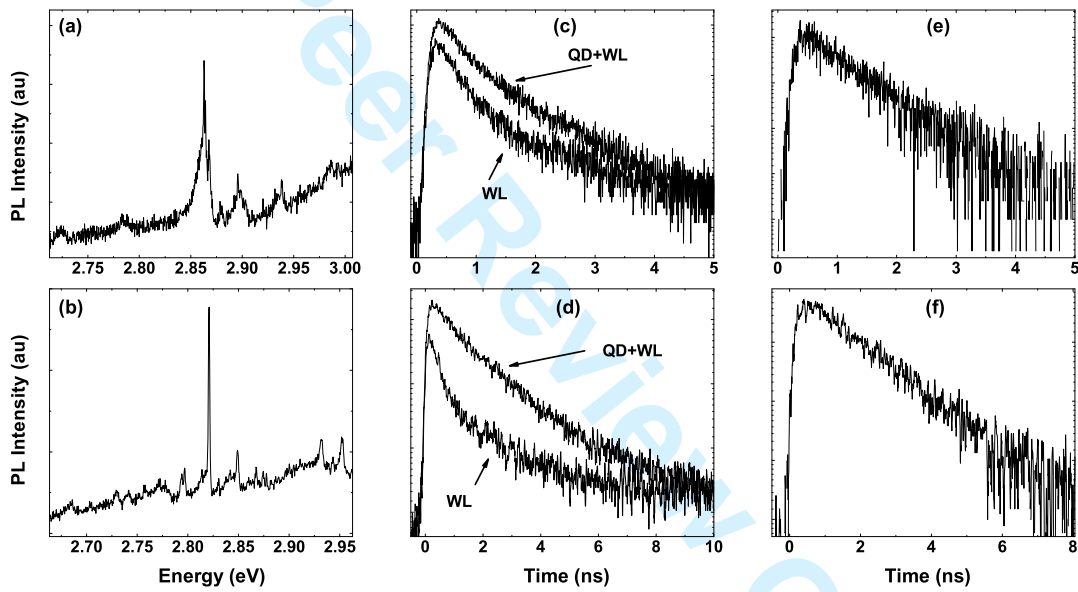


Figure 3

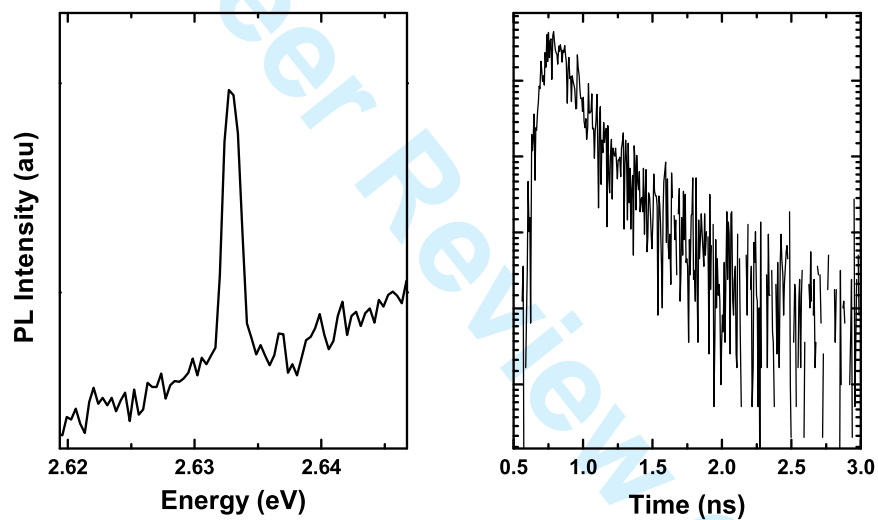


Figure 4

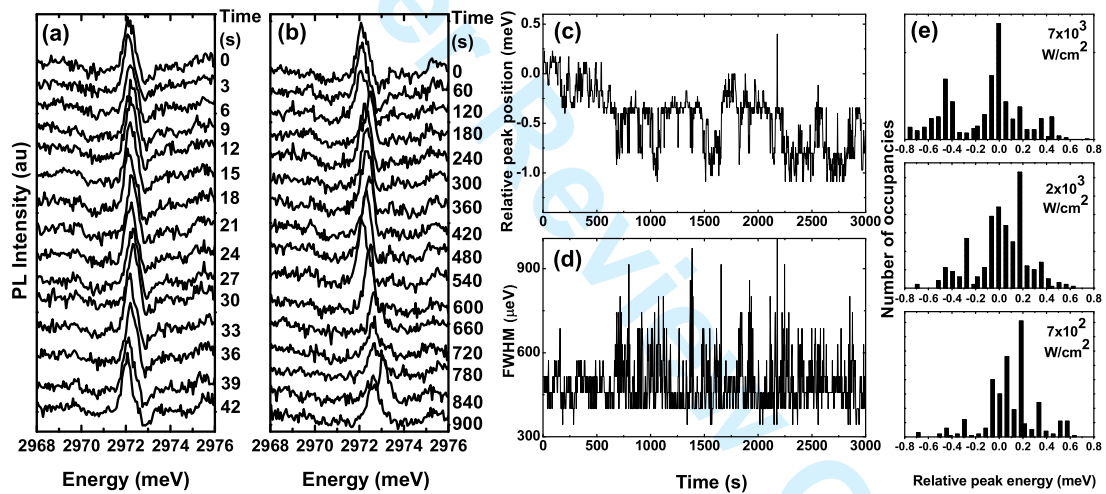


Figure 5

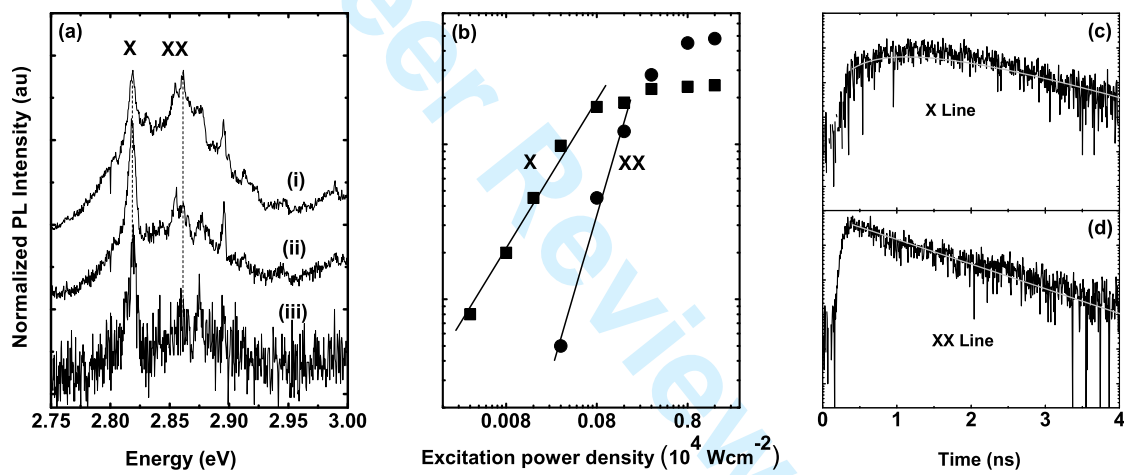


Figure 6

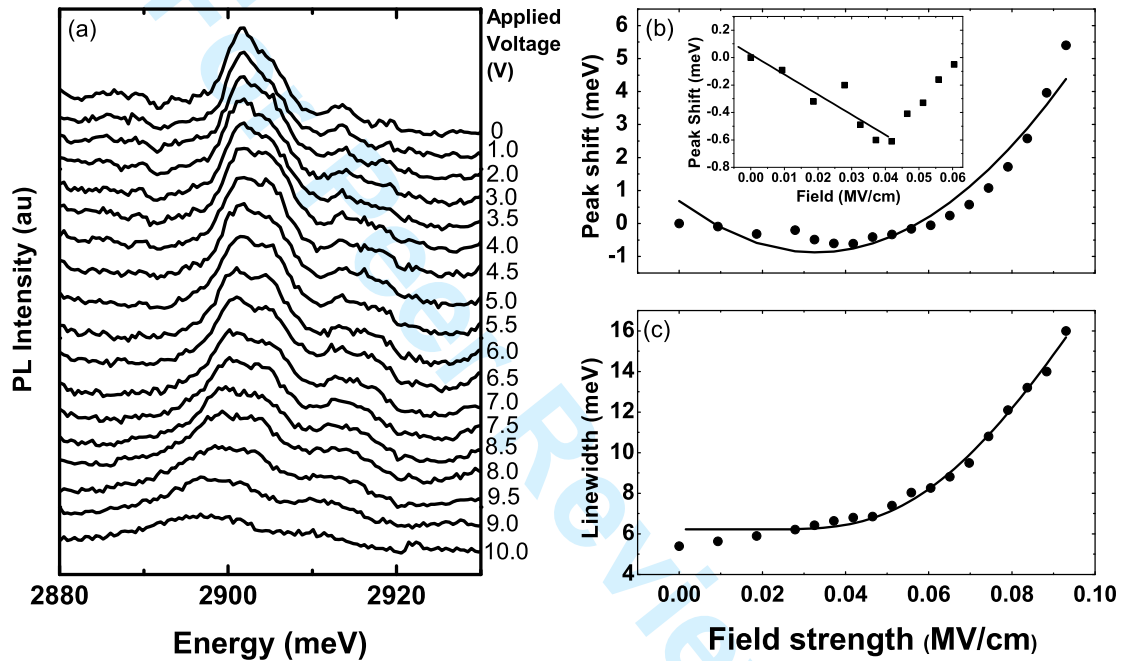


Figure 7

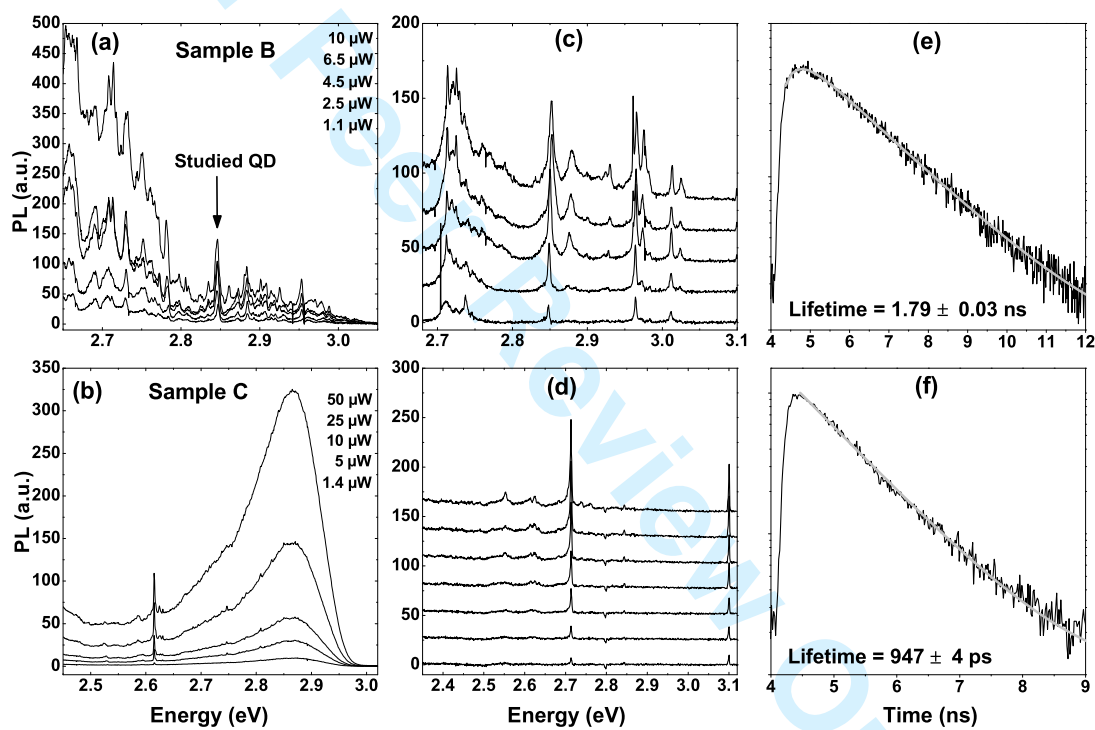


Figure 8

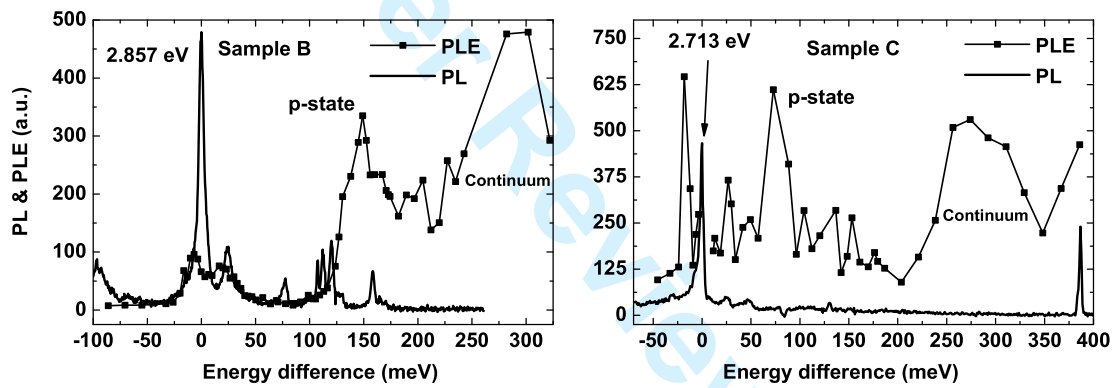


Figure 9

